Biophysical Journal
Article

Biophysical Society

Two-phase dynamics of DNA supercoiling based on DNA polymer physics

Biao Wan[1,*] and Jin Yu[2,*]
[1]Complex Systems Division, Beijing Computational Science Research Center, Beijing, China and [2]Department of Physics and Astronomy, Department of Chemistry, NSF-Simons Center for Multiscale Cell Fate Research, University of California, Irvine, California

ABSTRACT DNA supercoils are generated in genome regulation processes such as transcription and replication and provide mechanical feedback to such processes. Under tension, a DNA supercoil can present a coexistence state of plectonemic and stretched phases. Experiments have revealed the dynamic behaviors of plectonemes, e.g., diffusion, nucleation, and hopping. To represent these dynamics with conformational changes, we demonstrated first the fast dynamics on the DNA to reach torque equilibrium within the plectonemic and stretched phases, and then identified the two-phase boundaries as collective slow variables to describe the essential dynamics. According to the timescale separation demonstrated here, we developed a two-phase model on the dynamics of DNA supercoiling, which can capture physiologically relevant events across timescales of several orders of magnitudes. In this model, we systematically characterized the slow dynamics between the two phases and compared the numerical results with those from the DNA polymer physics-based worm-like chain model. The supercoiling dynamics, including the nucleation, diffusion, and hopping of plectonemes, have been well represented and reproduced, using the two-phase dynamic model, at trivial computational costs. Our current developments, therefore, can be implemented to explore multiscale physical mechanisms of the DNA supercoiling-dependent physiological processes.

SIGNIFICANCE DNA supercoiling is essential for a variety of cellular processes. Describing the supercoiling dynamics quantitatively is however challenging as the relevant timescale spans from submicroseconds to over seconds. In this work, based on the worm-like-chain model of DNA, we have developed a coarse-grained approach across timescales on modeling the supercoiling dynamics in two phases (plectonemic phase and stretched phase) that characterizes mechanical responses of supercoiling consistently with the worm-like-chain model but at trivial computational costs. The two-phase model further captures the plectonemic DNA nucleation, diffusion, and hopping measured experimentally. Our study thus supports biophysical approaches to reveal physiological mechanisms of DNA supercoiling.

INTRODUCTION

Supercoiling is ubiquitous in cellular DNA and results from the topology of double-helical DNA (1–5). For eukaryotic DNA, large structural domains ($\sim$ 1 Mb) emerge in the genome as the topologically associating domains (6–8), which are further divided into smaller supercoiling domains ($\sim 10^5$bp) (9–11). For the prokaryotic DNA, comparatively large structural domains and smaller supercoiling domains are also present (e.g., *E. coli* with several 10^4 bp and $\sim 10^4$ bp) (10,12). Supercoils are generated in many crucial genetic processes and in turn regulate corresponding processes, including transcription, replication, and genome condensation (2,13–19). During transcription elongation, an RNA polymerase (RNAP) moves along the helical DNA and generates twists, which subsequently create positive supercoiling ahead of the RNAP or downstream and negative supercoiling behind or upstream (13). The accumulation of the torsional stress can slow down or even stall the transcription elongation (14,15). Recent experiments show long-distance cooperative and antagonistic dynamics of multiple RNAPs via supercoiling (20), justifying the role of supercoiling as a long-range mediator (21). A previous modeling study pointed out that multiple RNAPs facilitate elongation by reducing collisions or traffic jam by torques (22); another model suggested that multiple RNAPs also induce strong supercoiling to bring significant transcription fluctuations (23). In addition, supercoiling contributes to the chromosome condensation (18,19), during which the negative supercoils accumulate in the protein-free region of the DNA (24). Under tension, the accumulative supercoiling

Submitted May 21, 2021, and accepted for publication January 5, 2022.
*Correspondence: wanbiao@csrc.ac.cn or jin.yu@uci.edu
https://doi.org/10.1016/j.bpj.2022.01.001

presents twisted and interwound coils called plectonemes, which may act as a driving force for compacting the chromatin fiber (24,25).

A supercoil can be partitioned into two parts, twist and writhe, which play distinct roles in genomic processes (26). Underwound DNA (with negative twists) can melt the secondary structures of DNA, and this can attract regulatory proteins (26–28). In contrast, overwound DNA (with positive twists) can hinder enzymatic activities associated with opening of the DNA duplex, such as in transcription initiation and elongation (14,15). On the other hand, writhe characterizes spatial crossings of DNA segments (3,29), accordingly facilitating distant interactions on DNA (30–33). Writhe can be in a solenoidal or a plectonemic form, or a combination of both. Under an external stretching force, supercoiled DNA can present a coexistence state of both forms (34–37), in which the plectonemic coils form the plectonemic (P) phase, whereas the solenoidal coils are almost straightly stretched, forming the stretched (S) phase (37,38).

DNA supercoiling has been quantitatively studied with single-molecule techniques (35,39–47). The extension-twist curves from experiments reveal a coupling between supercoiling (characterized by linking number) and DNA extension under stretching force (39–41). The discontinuities on torque or extension versus linking number were also observed in experiment (48). Experiments with a magnetic tweezer pulling fluorescently labeled DNA have directly detected the coexistence phase, and remarkably, measured the time-dependent supercoiling dynamics, e.g., plectoneme diffusion and hopping (46). The propagation of a plectoneme along DNA via diffusion presents the conformational rearrangement of DNA at about hundreds of base pairs per second. The hopping happens comparatively fast, and the fastest one observed takes tens of milliseconds for a displacement of thousands of base pairs (46). The surviving time of the individual plectoneme from nucleation to vanishing, i.e., the plectoneme lifetime, spans from milliseconds to several seconds.

Accompanying experiments, theoretical studies of DNA supercoiling have been developed based on the worm-like chain (WLC) model (37,49–52). The WLC model provides a description of the coupling between supercoiling and DNA extension (51,53), and it reveals the preplectonemic loops formed by bending DNA, or buckling transition (54), which give rise to the discontinuities on torque and extension versus linking number curves (55,56). Further, studies show that under a stretching force, the coexistence of the S and P phases is maintained under a coexistence torque that is a function of the stretching force (37).

Nevertheless, the related theories concern mostly the equilibrium and static behaviors, without elucidating the time-dependent dynamic processes. The experiments suggest that the dynamics of plectonemes essentially cover multiple timescales (46). In this study, we focus on building a DNA supercoiling model to describe these dynamic processes across the timescales.

Apart from the analytic theories, computational simulations and numerical methods have offered effective ways to probe supercoiling dynamics. Atomistic molecular dynamics (MD) simulations provide the finest details of such dynamics. For example, MD simulations of DNA mini-circles (10^2 bp) reveal writhe fluctuation and configuration diversity (57–59). To improve computational efficiency, a coarse-grained model that treats nucleotides as beads with three interaction sites, called oxDNA, was developed (60). Furthermore, by unitizing MD and the coarse-grained simulations, the multiscale dynamics of supercoiling have been studied (61,62). Nevertheless, computational costs of these models are high and the simulation timescales are limited by microseconds (63). The models without considering DNA sequence structure are capable of exceeding such a limit. An elasto-dynamic model (i.e., the Kircholff rod), for example, has been developed, by which DNA is characterized in terms of a continuum rod while omitting thermal fluctuations (64). The corresponding applications were carried out on supercoil removal (65) and on compressed DNA inside bacteriophage cavity to allow DNA ejection (66). In particular, for a representative polymer physics model, the numerical approach of the WLC model, i.e., the discrete worm-like chain (dWLC) method, has been widely implemented in simulating DNA with the thermal fluctuations incorporated (67). For example, the Monte Carlo (MC) simulations of the WLC model have been used in describing DNA thermodynamics, conformation, and site juxtaposition (33,68,69). The Brownian dynamics (BD) simulations, on the other hand, have been applied more widely in studying supercoiling (67,70). Such type of studies successfully show the plectoneme diffusion (71), supercoiling conformations (68,72), buckling transition (54,73,74), modeling DNA wrapped around a model histone (75), and supercoil removal by nicking (76). Besides, other semiflexible polymer models with Lennard-Jones potential have also been utilized to investigate the mechanism of supercoiling by rotating the ends (77) or using interwoven and braided polymers to produce plectonemes (38).

The computational costs of the aforementioned models are still significant for studying plectoneme dynamics. For example, by employing the dWLC method, simulating the plectoneme dynamics over a second requires weeks of CPU time (74,76). In this study, we developed a two-phase (S and P phases) dynamic model of DNA supercoiling at trivial computational cost based on the WLC polymer physics model. A primary task is to identify the fast dynamics comparing to the phase-transformation and possibly integrate them to reduce the degrees of freedom (78,79). Here we demonstrate first the dynamics and timescales of the torque transport within S and P phases that define the fast dynamics. Then we choose interphase boundaries as the slow dynamic observables and obtain the associated energetics.

Subsequently, we derive the Langevin dynamics of the slow observables. The results suggest that a DNA supercoil can quickly propagate as twist and slowly propagate as writhe (or plectonemes) along DNA. For calibration and consistency check, we compare the numerical results from the two-phase dynamic model with those from the dWLC method. For applications, we reproduce the supercoil dynamics on plectoneme diffusion, nucleation, and vanishing as being measured experimentally, together with the force or ionic strength dependency. Finally, plectoneme hopping and the associated energetics transformations between the two phases are also examined.

METHODS

In this section, we briefly summarize the method of construction of the two-phase dynamics for the coexistence state of the supercoiled DNA. If a system can be explicitly described by a fast variable **x** and a slow variable **X**, by averaging out **x**, the dynamic of **X** represents a coarse-grained description of the original system. By employing the dWLC method, dynamics faster than reaching the torque equilibrium within P and S phases are identified as fast or described by fast variable **x**. Interphase boundaries are identified as slow variable **X**. The Langevin equations of **X** describe the dynamics of plectonemes along DNA under topological and geometrical constraints. The parameters of the two-phase dynamics come basically from the WLC model. Furthermore, generating or removing plectonemes along DNA is based on the MC procedures: a plectoneme with the contour length of a loop can be introduced as a seed for plectoneme growing or shrinking depending on corresponding energetics and consequent weight or probability; a plectoneme with the contour length shorter than that of a loop can be deleted or preserved also depending on the system energetics and weight. Detailed information can be found in the Results and Supporting Material.

RESULTS

Fast torque equilibrium can be reached within the stretched and plectonemic phases

Torque transport on stretched DNA or S phase

We study the dynamics of torque propagation on supercoiled DNA based on the WLC model numerically, i.e., via an implementation of the dWLC method (see Text S1). The source code is available at https://doi.org/10.6084/m9.figshare.16685689. First we have analytically explored the dynamics of torque transport along DNA.

In the WLC model, harmonic potentials are used in representing the elasticities of DNA (2,50,70). The twist energy density is defined as

$$\mathcal{E}_{twist} = \frac{1}{2} k_B T l_t \left(\frac{\Delta\theta}{\Delta u}\right)^2 \tag{1}$$

where k_B is the Boltzmann constant, T is the room temperature, l_t is the torsional persistence length, i.e., $l_t = 75$ nm, and $\Delta\theta$ is the twist on the segment Δu. We introduce an internal torque T_q^{in} as a measure of torsional stress on DNA, $T_q^{in} \equiv k_B T l_t \frac{\Delta\theta}{\Delta u}$. Based on the elastic properties of DNA, the torque transport along DNA can be written as follows (see Text S2):

$$\frac{\partial T_q^{in}}{\partial t} = \frac{l_t k_B T}{\zeta_R} \frac{\partial^2 T_q^{in}}{\partial u^2}, \tag{2}$$

where the drag coefficient for a rotational cylinder $\zeta_R = 4\pi R^2 \eta$, the radius of DNA $R = 1$ nm, and the viscosity $\eta = 0.001$ kg/m/s). A solution to Eq. 2 can be found in Text S2. The time for torque to reach equilibrium is at $2.5 \frac{\zeta_R}{l_t k_B T} L^2$ (about 0.1 ms for 3000 bp) (Text S2), independent of stretching force, torque, and linking number. For example, a twist pulse starting at one end of the stretched DNA or S phase will spread over 10^3 bp within 10^{-2} ms and 10^4 bp within 1 ms.

Fig. 1 *a* shows the scheme for simulating the torque transport on stretched DNA using the dWLC method. Under a constant stretching force $f = 0.4$ pN, DNA is twisted by an external torque $T_q^{ex} = 9$ pNnm starting at $t = 0$ ($T_q^{ex} = 0$ at $t<0$). After that, the torque is kept constant and the torsional response of DNA is monitored.

The curves in Fig. 1 are all averaged over 20-simulation trajectories. After being initially twisted, the mean internal torque, $\overline{T}_q^{in}$, reaches equilibrium (9 pNnm) at about 0.03 ms for 1500 bp and about 0.1 ms for 3000 bp, consistent with the estimation above. As Eq. 2 describes the mechanical properties of DNA, the curves in Fig. 1 *b* are averages over stochastic trajectories.

Supercoiling can be quantified by the excess linking number ΔLk or the linking number density σ (see Text S3). The free energy density of a stretched DNA at equilibrium is $\mathcal{F}_S = \frac{1}{2} c_S (\sigma_S^{eq})^2 + \mathcal{F}_0$ (Text S4), including the contributions from torsion and force stretching (37,53), where c_S stands for the torsional stiffness, which is a function of force f, the DNA torsional persistence length $l_t = 75$ nm, and the DNA bending persistence length $l_b = 50$ nm ; σ_S^{eq} is the equilibrium linking number density of the stretched phase, and $\mathcal{F}_0$ is the free energy density without torsion or equivalent force (49). At equilibrium, the torque is defined as $\frac{1}{\Omega_0} \frac{\partial \mathcal{F}_S}{\partial \sigma_S^{eq}}$(37), where the constant $\Omega_0 = 1.85\text{nm}^{-1}$ is the rotation angle of the DNA backbone per unit length (2,37). Thus, we have

$$\sigma_S^{eq} = \frac{\Omega_0 T_q^{in}}{c_S}. \tag{3}$$

We accordingly obtained computationally the excess linking number density of the stretched DNA as shown in Fig. 1 *c*. σ_S reaches the equilibrium value at 0.03 ms for 1500 bp and 0.1 ms for 3000 bp. Fig. 1 *b* and *c* suggest a synchronized equilibrium process in the S phase in 0.1 ms.

Torque transport on plectoneme or P phase

A plectoneme can be considered a pair of rods antiparallel, interwound around each other under a torsional constraint (37,80). Thus, an empirical form of the energy of the

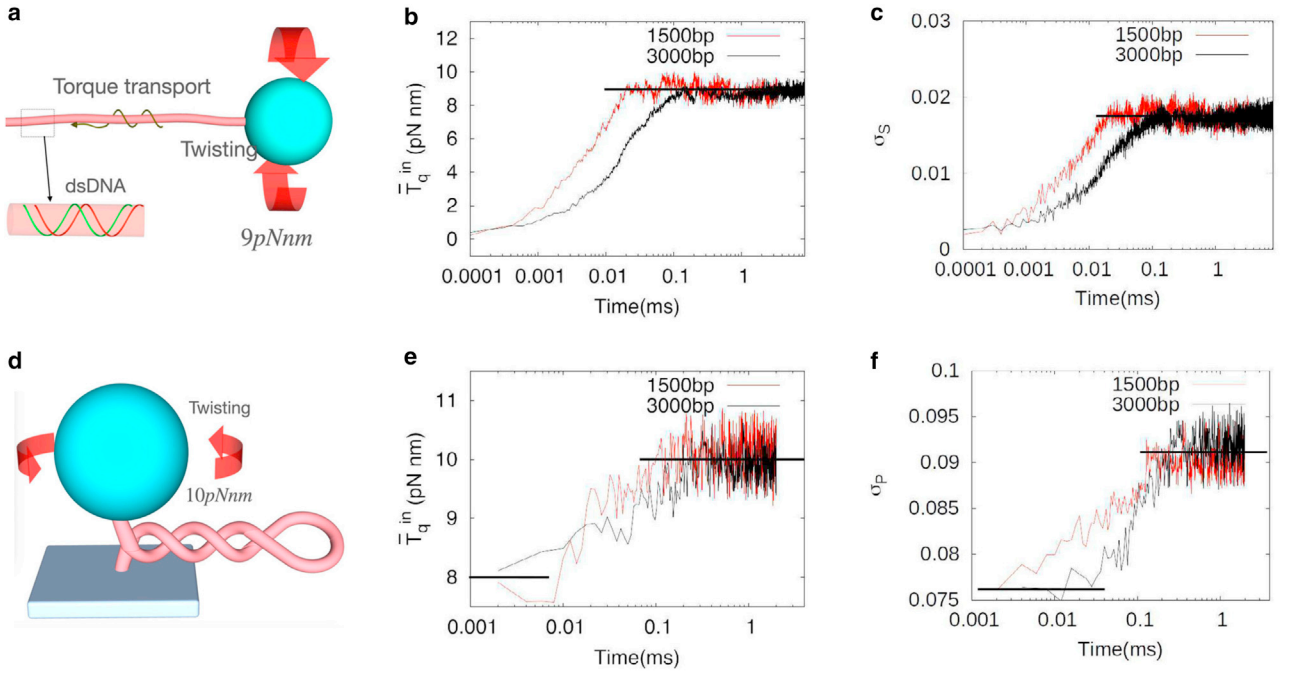

FIGURE 1 Torque transport on the stretched (S) phase and the plectonemic (P) phase of the supercoiled DNA based on the dWLC method. (*a*) The schematic of the torque transport along the S phase after an external torque T_q^{ex} promptly applied from 0 to 9 pNnm at $t = 0$. (*b*) The internal torques averaged over 20 trajectories. $\overline{T}_q^{in}$ rises to equilibrium within 0.1 ms to follow T_q^{ex}. (*c*) The excess linking number density σ_S reaches to equilibrium within 0.1 ms. (*d*) The schematic shows that a pure plectonemic DNA follows a promptly applied torque, T_q^{ex}, from 8 pNnm (t<0) to 10 pNnm at $t = 0$. The internal torque along DNA consequently propagates on the plectoneme. (*e*) The mean torque of DNA, $\overline{T}_q^{in}$, reaches equilibrium (10 pNnm) within 0.3 ms. (*f*) The excess linking number density σ_P reaches equilibrium value within 0.3 ms.

plectoneme, $\mathcal{F}_P = \frac{1}{2}c_P\sigma_P^2$, can be utilized (37,69,80), where $c_P \equiv l_p k_B T \Omega_0^2$ is the torsional stiffness of plectoneme, l_p is the torsional persistence length of the plectonemic helix, depending on the ionic strength and often taking value of 21–27 nm (80), and σ_P is the excess linking number density of the plectonemes. The internal toque is defined similarly as that of the stretched DNA, i.e., $c_p\sigma_P/\Omega_0 = T_q^{in} = k_B T l_p \frac{\Delta\Theta}{\Delta u}$, and here we have introduced a plectonemic twist Θ (see Fig. S11), similar to θ in Eq. 1. The twist energy density is

$$\mathcal{E}_{twist}^{P} = \frac{1}{2}k_B T l_p \left(\frac{\Delta\Theta}{\Delta u}\right)^2. \tag{4}$$

We consider the torque transport on a plectoneme as the propagation of the plectonemic twist, i.e.,

$$\frac{\partial T_q^{in}}{\partial t} = \frac{l_p k_B T}{\zeta_P}\frac{\partial^2 T_q^{in}}{\partial u^2}, \tag{5}$$

where $\zeta_P \approx 2\pi R_{plect}^2 \eta$ is the drag coefficient due to motions of the two parallel rods, and R_{plect} the radius of plectonemes (46,81), about 2.5 nm. The time for torque equilibrium on a plectoneme with contour length L can be calculated as $2.5\frac{\zeta_P}{l_p k_B T}\left(\frac{L}{2}\right)^2$, about 0.26 ms for torque equilibrium for 3000 bp.

Fig. 1 *d* illustrates the setup of torque transport on a pure plectoneme, which is originally maintained by a preexisting external torque $T_q^{ex} = 8$ pNnm (t<0). Then the external torque jumps to $T_q^{ex} = 10$ pNnm at $t \geqslant 0$, and the ensuing torsional response of the plectoneme is monitored.

The mean internal torques of plectonemes are shown in Fig. 1 *e*. After the torque jumping at $t = 0$, the mean internal torques, $\overline{T}_q^{in}$, rise from 8 pNnm to 10 pNnm at about 0.1 ms and 0.3 ms for 1500 bp and 3000 bp, respectively, as estimated earlier.

We also numerically monitored the excess linking number density of the plectoneme as shown in Fig. 1 *f*. The equilibrium torque is defined as $\frac{1}{\Omega_0}\frac{\partial \mathcal{F}_P}{\partial \sigma_P^{eq}}$. Thus,

$$\sigma_P^{eq} = \frac{\Omega_0 T_q^{in}}{c_P}. \tag{6}$$

As Eq. 6 suggests, $\sigma_P^{eq} = \frac{T_q^{ex}\Omega_0}{c_P} = 0.076$ at t<0. Subsequently, σ_P reaches a new equilibrium defined by $\frac{T_q^{ex}\Omega_0}{c_P} = 0.091$ at about 0.1 ms for 1500 bp and 0.3 ms for 3000 bp.

The torque equilibrium (Eqs. 3 and 6) inside the S and P phases can be applied to their coexistence state, meaning $c_P\sigma_P^{eq} = c_S\sigma_S^{eq}$ at the phase boundary. Next, we show that the phase boundaries can be chosen as the slow observables to quantify the plectoneme dynamics.

Two-phase dynamics of DNA supercoiling

We have demonstrated the submillisecond dynamics of torque to reach equilibrium within the S and P phases. The intra-phase equilibrium defines the fast dynamics, and then can be averaged out within the two phases when interphase boundaries are considered as slow variables. We show subsequently that the energy gradients at the phase boundaries drive the transformation between the two phases and thus establish a two-phase dynamic model for describing the DNA supercoiling.

Interphase boundaries as slow observables

Multiple plectonemes have been observed in the extended DNA supercoil in experiment (46), and the timescales of corresponding dynamics span from millisecond to second. The dynamics of the plectonemes can be described by the boundaries between the S and P phases. We therefore label the plectonemes from the fixed end to the stretching end with $\alpha = 1, 2, \ldots$ (Fig. 2 *a*). $\mathbf{X} \equiv (X_\alpha^l, X_\alpha^r)$ are the boundaries of plectonemes, where the superscripts l and r denote the left and right boundaries of the α-th plectoneme, respectively. Along the axis, $X_\alpha^l < u \leqslant X_\alpha^r$ locates the α-th plectoneme, and $X_{\alpha-1}^r < u < X_\alpha^l$ specifies the α-th section of the S phase. The formation of plectonemic coils can make DNA compact by bringing distant sites together, i.e., X_α^l and X_α^r are in physical contact. Plectoneme propagation corresponds to the movement of X_α^l and X_α^r in the same direction. For example, in Fig. 2 *b*, if the α-th plectoneme moves left, the S phase on the left-hand side of X_α^l is transformed into the P phase, and the P phase on the left-hand side of X_α^r is transformed into the S phase. This process is accompanied with the internal slithering of parallel segments of the plectonemic helix (Fig. 2 *b*).

The separation of timescales of torque equilibrium (intra-phase) and phase boundary (interphase) has been numerically justified in Text S5, e.g., torque relaxation in 0.02 ms for DNA at 3000 bp, and relaxation of the phase boundary in 1.5 ms. The separation of timescales of the fast and slow dynamics are well defined if $L < 10$ μm (3×10^4 bp). For DNA longer than 10^4bp, supercoiling domains may emerge (10,12). Accordingly, the two-phase dynamics is valid inside the domain (see Text S6).

During transcription elongation on DNA of thousands of base pairs, RNAP synthesizes per nucleotide on the order of 10 ms or longer (23,82). The intra-phase torque equilibrium is reached (within submilliseconds), and the interphase boundaries are also relaxed (in milliseconds). Thus, supercoiling accumulations during transcription can be regarded as quasi-static processes.

Free energy associated with the slow observables

With separation of the timescales, one can average out the fast dynamics within P and S phases and keep the torque equilibrium to characterize the dynamics of the phase boundary. On such a timescale, the torque equilibrium at the boundaries means $c_P \sigma_P^{eq} = c_S \sigma_S^{eq}$. Accordingly, every plectoneme carries an equal σ_P^{eq}. The free energy density of each plectoneme is therefore represented as $\mathcal{F}_P(\mathbf{X}) = \frac{1}{2} c_P (\sigma_P^{eq})^2$ (69,80).

The translational displacement of the α-th section of the S phase is subject to the viscous drag along it. At $u < X_\alpha^r$ and $> X_\alpha^l$, the force imposed on DNA is f_u, and at the stretching end, $f|_{u=L} = f$. The local free energy density (or force) is represented by $\mathcal{F}_S(u, \mathbf{X}) = \frac{1}{2} c_S (\sigma_S^{eq})^2 + \mathcal{F}_0$ (37,53).

The free energy associated with $\mathbf{X}$ can be written as the contributions from the S and P phases:

$$\Phi_0(\mathbf{X}) = \sum_{\alpha=0} \int_{X_\alpha^r}^{X_{\alpha+1}^l} \mathcal{F}_S(u, \mathbf{X}) du + \sum_{\alpha=0} \int_{X_{\alpha+1}^l}^{X_{\alpha+1}^r} \mathcal{F}_P(\mathbf{X}) du. \tag{7}$$

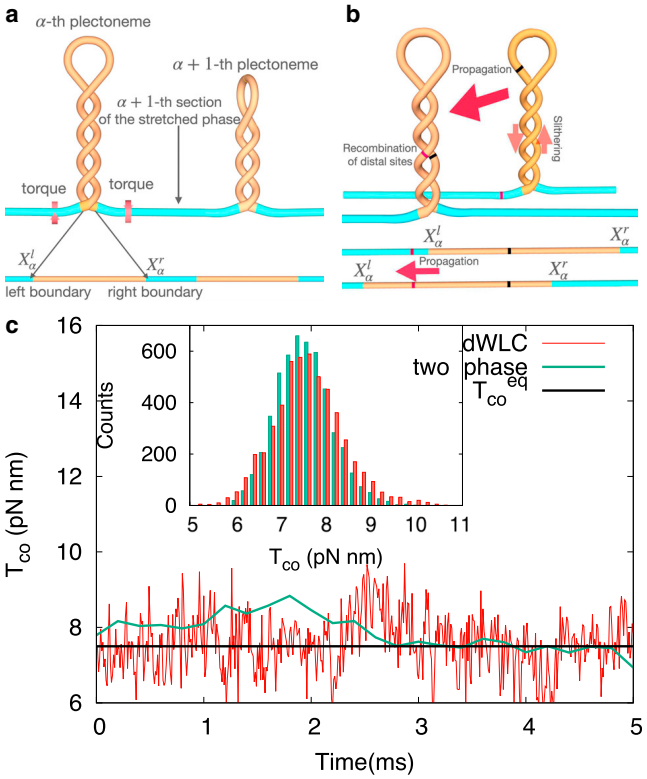

FIGURE 2 Two-phase dynamic model of DNA supercoiling. (*a*) The schematic of the α-th plectoneme among multiple plectonemes, showing the torque equilibrium between the plectoneme (P) and stretched (S) phases. By mapping the P and S phases into a one-dimensional arc-length parameter space, one can introduce $u = X_\alpha^l$, the left boundary of the α-th plectoneme, and $u = X_\alpha^r$, the right boundary of the α-th plectoneme. (*b*) The propagation of the α-th plectoneme. The slithering of the segments of the plectonemic helix facilitates the recombination of distal sites on DNA (marked by red and black marks). (*c*) Simulation trajectories based on the WLC model and the two-phase dynamics. The coexistence torque of a DNA of 4500 bp at $f = 0.5$ pN fluctuates around the static coexistence torque, T_{co}^{eq}. The histograms in the inset show coexistence torque obtained from the dWLC simulations (red bars, 50 ms in total) and that from the simulations using the two-phase dynamic model (green bars, 1 s in total). The torque obtained from the two-phase model can be regarded as being smoothed from the dWLC method.

Langevin dynamics

The slow variables $\mathbf{X}$ then evolve under the driving force from the free energy Eq. 7. The gradient $\nabla_{\mathbf{X}}\Phi_0(\mathbf{X})$ serves as a driving force, driving the transformation between S and P phases. The variables $\mathbf{X}_\alpha^{l/r}$ thus follow the Langevin equations:

$$\dot{X}_\alpha^{l/r} = -\frac{1}{\gamma_\alpha}\nabla_{X_\alpha^{l/r}}\Phi_0(\mathbf{X}) + \sqrt{\frac{2k_BT}{\gamma_\alpha}}\dot{W}, \tag{8}$$

where γ_α is drag coefficient for the growth or shrinkage of the α-th plectoneme (see Text S6). It should be noted that Eq. 8 should apply with two constraints: the first one is the topology constraint ($\Delta Lk = \Delta Lk_S + \Delta Lk_P$; see Text S3 for the additivity), and the second one is the inextensibility (geometry constraint) of DNA ($L = L_S + L_P$) (see Text S6). The source code is available at https://doi.org/10.6084/m9.figshare.16685689.

The equilibrium point, i.e., $\nabla_{X_\alpha^{l/r}}\Phi_0(\mathbf{X}) = 0$, leads to the static coexistence torque $T_{co}^{eq} = \frac{1}{\Omega_0}\left(\frac{2c_P\left(f-\sqrt{\frac{k_BTf}{l_b}}\right)}{1-c_P/c_S}\right)^{\frac{1}{2}}$ (37).

Actually, the dynamics of the slow variables $\mathbf{X}$ accompany with a time-dependent coexistence torque, $T_q^{co}(t) \equiv \frac{c_P\sigma_P^{eq}(t)}{\Omega_o}$ (Fig. 2 *c*). The torque of DNA at length of 4500 bp under $f = 0.5$ pN fluctuates around T_{co}^{eq}. Fig. 2 *c* suggests that although the fluctuations faster than the torque equilibrium have been averaged out, the mean and the variance of the torque are still consistent with those obtained from the dWLC method (inset in Fig. 2 *c*). Thus, the two-phase dynamic model can be regarded as a smoothed version of the dWLC method.

For supercoiling under externally constant torque, the free energy densities can be obtained through the Legendre's transformation $\mathcal{F}_{S/P}(T_q^{ex}) = \mathcal{F}_{S/P} - \Omega_0 T_q^{ex}\sigma^{eq}$. The free energy densities of the plectonemes and the stretched phase are therefore $\mathcal{F}_P = -\frac{1}{2}\frac{(\Omega_0 T_q^{ex})^2}{c_P}$ and $\mathcal{F}_S = -\frac{1}{2}\frac{(\Omega_0 T_q^{ex})^2}{c_S} - f_u + \sqrt{\frac{k_BTf_u}{l_b}}$, respectively. Inserting them into Eqs. 7 and 8, we obtained the dynamic model of extended DNA supercoiling under constant torque.

Comparing with the WLC model

In this section, by employing the dWLC method, we compare and calibrate the two-phase dynamic model via two examples. One is the supercoiling accumulation at a constantly twisting rate. The other one is supercoiling accumulation under a constant torque. We show that the two-phase dynamic model at trivial computational costs provides consistent results with the dWLC method. In the second case, plectonemes finally dominate the supercoiling state under an external torque larger than T_{co}^{eq}. This nonequilibrium process helps determine the slithering drag coefficient by calibration.

Supercoil accumulation and buckling transition at a constant rate

An extended DNA undergoes linking number accumulation when one end of the DNA is rotated while the other end is kept fixed, as shown in Fig. 3 *a*. The stretching force $f = 0.5$ pN, the rotation angle $\Omega = \omega t$, and the angular velocity $\omega = 20\pi/s$, equivalent to $\Delta Lk = 10$ per second (i.e., comparable to polymerase enzyme unwinding and synthesizing at 100 nucleotides or nt per second) (23,82). At first, the extended DNA is twisted, and then it undergoes a buckling transition (discontinuities on torque and extension curves) followed by plectoneme formation (48).

Curves in Fig. 3 *b* are averaged over 4-simulation trajectories. The relative extension z/L almost remains unchanged before 0.6 s while the torque gradually builds up, suggesting that the extended DNA is twisted. The buckling indeed marks the starting point of the phase coexistence and indicates the extension and torque switch between two distinct values, giving rise to the discontinuities (55,83). These important features have also been captured previously in single-molecule experiment (48). After that, the torque drops and converges as torsional stress on DNA is relieved, indicating that the excess twist is transformed into writhe. The coexistence torque remains unchanged when more linking number is injected.

We noticed that the computational cost of the dWLC in the plectonemic phase is still significant and grows linearly with the contour length in the P phase (Text S7). The two-phase dynamic model, however, reduces the computational cost by several orders of magnitude because only slow dynamics are examined. In Fig. 3 *c*, the torque and extension curves (averaged over 50 trajectories) generated from the two-phase dynamic model well reproduce those in Fig. 3 *b* from the dWLC method and are consistent with previous studies (48,74).

We have justified the quasi-static process of DNA supercoiling accumulation at $\Delta Lk = 0.1$ per 10 ms. Thus, the above torque or extensive curves depend on the mechanical parameters l_b, l_p, and l_t, which may vary under solution and other experimental conditions (14,48,49,55,76,80,84). Sensitivity analysis for torque and extension curves by varying these parameters can be seen in Text S8. In brief, one can see that before buckling, torque and extension curves are insensitive to changes on bending persistence length of DNA, l_b, and torsional persistence length of plectoneme, l_p, but sensitive to torsional persistence length of DNA, l_t, although the coexistence torque is insensitive to l_b and l_t, but sensitive to l_p (see Eq. 4).

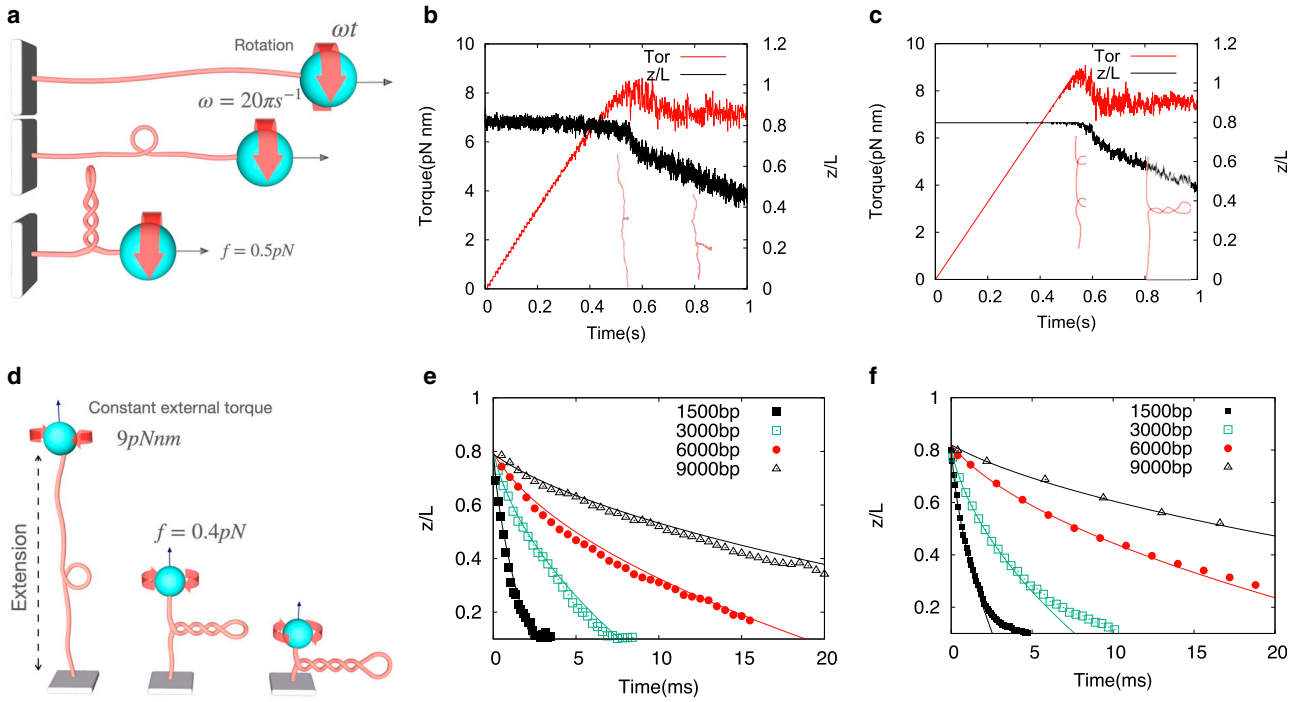

FIGURE 3 Torque and extension curves in buckling transition and extension curves of the DNA during supercoil accumulation. (*a*) Injecting supercoil (i.e., increasing linking number) at constant rate to the DNA of 3000 bp within 1 s. The rotation rate ω is 20 π per second. (*b*) The torque (red curve) and relative extension z/L (black curve) obtained from the BD simulations based on the dWLC as the DNA is gradually twisted. (*c*) The torque and extension curves from (*b*) are reproduced using the two-phase dynamic model. (*d*) Injecting supercoil under a constant external torque, $T_q^{ex} = 9$ pNnm. (*e*) The relative extension from the BD simulations based on the dWLC with various DNA lengths. (*f*) The results from (*e*) are reproduced using the two-phase dynamic model. The curves in (*e*) and (*f*) are the fitting functions $\sqrt{1+\lambda t}$ (see Text S7).

Supercoil accumulation under a constant torque

In the two-phase dynamic model, all but the slithering drag coefficients are given based on the hydrodynamics of the WLC model (see Text S6). There is a factor in slithering drag coefficient μ_{slt} that can be determined by calibrating with the dWLC method. Fig. 3 *d* illustrates an extended supercoil under a constant torque, $T_q^{ex} = 9$ pNnm (comparable to 5 to about 11 pNnm torque exerted by polymerases (14)), and a constant stretching force $f =$ 0.4 pN. Since the external torque is larger than T_{co}^{eq} (i.e., 6.5 pNnm that maintains the coexistence state under 0.4 pN), plectonemes are created and the ultimate equilibrium state is dominated by plectonemes. Consequently, plectonemic coils build up until all stretched DNA is interwound to plectonemic coils.

Using the dWLC method, we can capture the dynamics of the plectoneme growth. Fig. 3 *e* shows the relative extensions z/L (averages over 20-simulation trajectories) of DNA at 1500, 3000, 6000, and 9000 bp. Indeed, the shrinking extensions indicate the growth of plectonemes. The fitting curves are generated using $\frac{z}{L} - \frac{z_0}{L} \propto 1 - \sqrt{1+\lambda t}$, where λ is a fitting parameter. We performed the simulations using the two-phase dynamic model shown in Fig. 3 *f* (averages over 50-simulation trajectories). The slithering drag μ_{slt} was then determined via λ (Text S8). Consequently, we can then reproduce the plectoneme dynamics.

Reproducing experimentally measured plectoneme dynamics

Previous experimental studies show that the plectonemes can diffuse and hop along DNA (46). Particularly, a hop event associates a plectoneme shrinking and vanishing at one position and a new nucleation at another remote position. By employing the two-phase dynamic model, we reproduced the plectoneme dynamics, including plectoneme diffusion, hopping, and associated lifetime.

Reproducing plectoneme diffusion

The interphase boundaries in the two-phase dynamic model can be used to monitor the plectoneme dynamics. Fig. 4 *a* shows a kymograph, i.e., the spatial versus time evolution process of the plectonemes of a 21-kbp (7 μm) DNA (extended under a force $f = 0.8$ pN and with $\Delta Lk = 70$), illustrating the coexistence of multiple plectonemes, and the plectoneme nucleating or vanishing, analogous to that shown in experiment (Fig. 1 *D* in van Loenhout et al. (46)).

Simulations of a plectoneme with one-fourth of the DNA contour length under different forces have been performed.

To estimate the diffusion constant, we calculated the mean-square displacement (MSD) $\overline{\Delta x^2(t)}$ of the plectoneme. As shown in Fig. 4 *b*, we obtained the diffusion constants via $D \equiv \frac{\overline{\Delta x^2(t)}}{2t}$ under different stretching forces. For consistency check, we also compared the results with the Einstein relation, i.e., $D = \frac{k_B T}{\zeta_{diff}}$, where ζ_{diff} is a sum of the viscous drags for the transverse displacement of the plectoneme (see Text S6). The diffusion constant of the plectoneme is about 10^{-1} $\mu m^2/s$, and the same magnitude was previously obtained from the hydrodynamic model (Fig. 3 *F* in van Loenhout et al. (46).)

Reproducing plectoneme hopping and computing the associated nucleation rate and lifetime

Hopping is accompanied with plectoneme shrinking and nucleation. Nucleation is affected by stretching forces and ionic strengths. The simulations of the P phase with one-fourth of the DNA contour length have been performed in the condition where the stretching force $f = 0.4$, 0.8, 1.6, and 3.2 pN. Large stretching force results in more compact plectonemes, i.e., reduces the radius of the plectonemic helix (Fig. 4 *c*). Indeed, in the coexistence state of DNA supercoiling, the equilibrium excess linking number density of the P phase is $\sigma_P^{eq} \sim \sqrt{f/l_p}$(37), which suggests that σ_P^{eq} increases with f.

At high salt concentration, the screening of the Coulomb repulsion potential reduces the effective repulsive DNA diameter, shortening torsional persistence length of the plectoneme l_p and radius of the plectonemic helix (80). Meanwhile, based on the coexistence state relation $\sigma_P^{eq} \propto \sqrt{f/l_p}$, lowering l_p increases the σ_P (Fig. 4 *d*). Accordingly, we adjust the torsional persistence length of plectoneme l_p to represent the impacts from the ionic strength (80), specifically, $l_p = 25$, 23, and 21 nm to represent the low, regular, and high salt concentrations, respectively. Nucleation rates obtained from simulations (Fig. 4 *e*) suggest that large stretching forces f and the high salt concentrations (small l_p) can suppress the nucleation events. Similar results on the nucleation rate have been previously detected in experiment (Fig. 4 *D* in van Loenhout et al. (46)). We phenomenologically derive a nucleation relation (Text S9):

$$k_{nuc} \propto exp\left(-2\sqrt{f}\, C\left(l_p^{\star} - l_p\right)\right), \tag{9}$$

where C and $l_p^{\star}$ are fitting parameters (dashed curves in Fig. 4 *e*). As $l_p \to l_p^{\star}$ (salt concentration decreases), the nucleation rate increases. That is because low salt concentration increases the radius of the plectonemic helices, then lower the energy penalty from plectonemic helix to loop. By fitting, we obtained $l_p^{\star} = 27$ nm.

The surviving time of the individual plectoneme from nucleation to vanishing is defined as plectoneme lifetime. Fig. 4 *f* shows that the mean lifetime τ_{plec}, spanning from 0.1 to 1 s, depends on stretching force and salt concentration, although most plectonemes are short lived (<0.1 s; see Fig. S10 *b*), consistent with that observed in experiment (Fig. 4 *E* in van Loenhout et al. (46)). The large f or small l_p increases the plectoneme lifetime. As discussed earlier, large f or small l_p lowers the plectoneme nucleation and also leads to more compact plectonemes. The resulting compactness stabilizes plectonemes, causing long mean lifetime of the individual plectoneme. By balancing the plectoneme nucleation rate and vanishing rate, we can derive the mean lifetime of the individual plectoneme (see Text S9):

$$\tau_{plec} \propto (2l_t - l_p) f exp\left(C\sqrt{f}\left(l_p^{\star} - l_p\right)\right), \tag{10}$$

where C and $l_p^{\star}$ are the same as those in Eq. 9.

An example of hopping over 10 kbp within about 0.1 s is shown in Fig. 4 *g*, similar to the kymograph constructed from experiment (Fig. 4 *B* in van Loenhout et al. (46)). Compared with movement of a plectoneme via diffusion, which scales with time as $t^{1/2}$, we observed that plectoneme hopping distance scales linearly with hopping time (Fig. 4 *h*), consistent with the estimation in the SI of van Loenhout et al. (46). Hopping time is defined as the time interval from the nucleation of the new plectoneme to vanishing of it (Fig. 4 *g*). Longer hopping distance requires longer time to rearrange the DNA conformation. A plectoneme with contour length 1.75 μm (5200 bp), diffuses $\sqrt{2Dt} \sim 0.6$ μm within 1 s for $D = 0.2$ $\mu m^2/s$. A plectoneme, however, can hop 2 to about 3 μm (10^4bp) per second, on average. Thus, plectoneme hopping offers several times faster conformational rearrangements on DNA than the plectoneme diffusion.

We also found that plectoneme hopping is associated with significant energy exchanges between the two phases. We identify the nucleation as the starting point of a hopping event. Then we collected up to 5000 simulations that contain the hopping events and aligned the starting points of the hopping events together for averaging the energetics. The energy change of the S phase accumulates up to about $20k_BT$ before the nucleation, whereas that of the P phase falls to about $-20k_BT$. These significant energetic changes facilitate the abrupt nucleating to vanishing processes (Fig. 4 *i*). After the formation of the new plectoneme by nucleation, the energetic changes rapidly converge to zero. The energetic offsets between the two phases indeed make the total energy change as small as thermal fluctuations, i.e., $1k_BT$ (inset of Fig. 4 *i*). It should be noted that there is no persistent energetic injection into the system.

DISCUSSION AND CONCLUSION

In this study, based on the polymer physics or the WLC model of DNA, we have constructed a two-phase dynamic

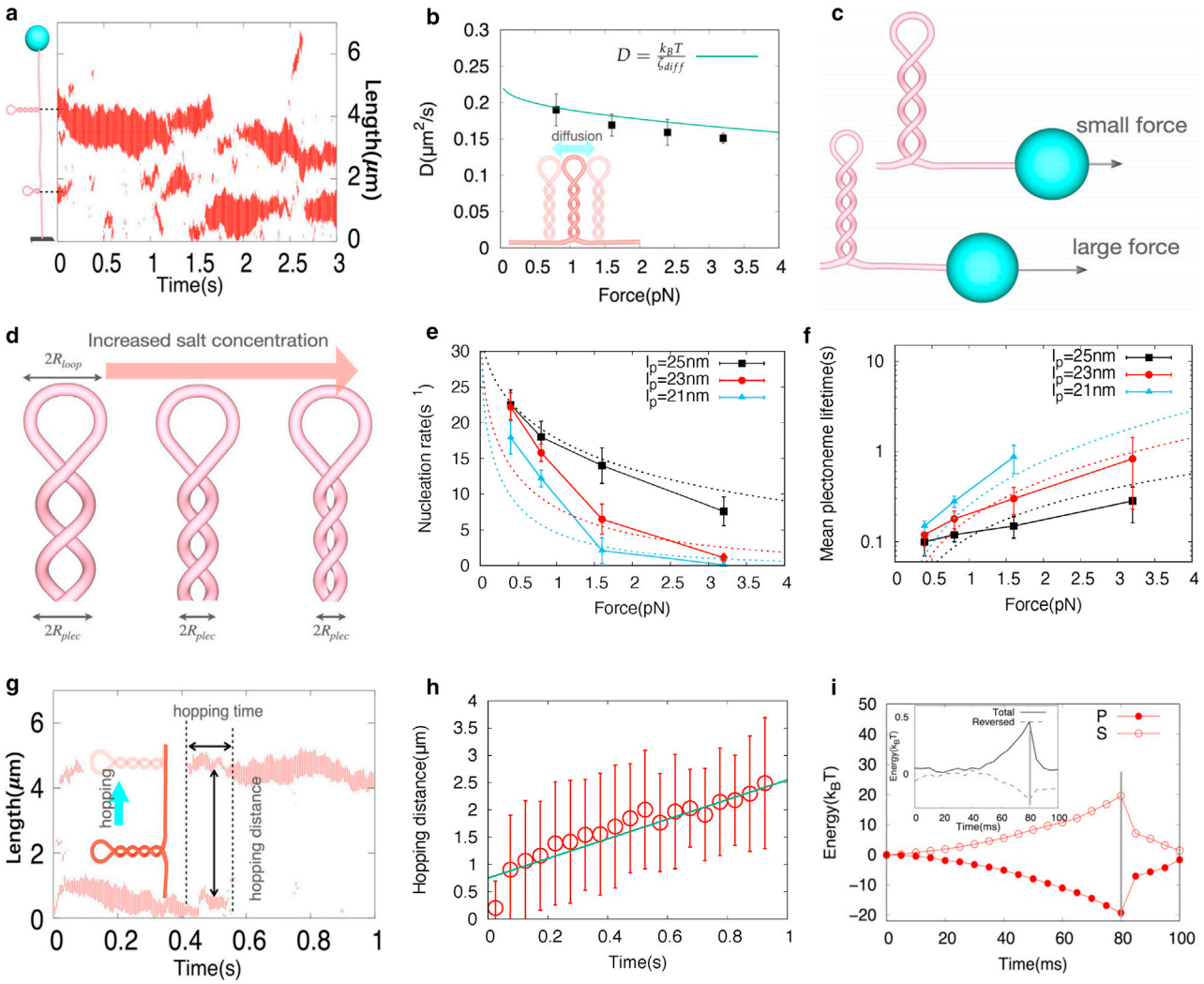

FIGURE 4 Obtaining plectoneme dynamics using the two-phase dynamic model. (*a*) The kymograph of the plectonemes of 21 kbp (7 μm) under a constant stretching force $f = 0.8$ pN and with a constant linking number $\Delta Lk = 70$. (*b*) The diffusion coefficients of a single plectoneme under different forces obtained from the simulations of the two-phase model (the dots). The error bars represent the standard deviation (SD) from 10 sets of 200 samples. The green curve is directly from the Einstein relation. In comparison, the diffusion constants predicted from the previous hydrodynamic model are 0.1–0.3 $\mu m^2/s$ (Fig. 3 *F* in van Loenhout et al. (46)). (*c*) Large stretching force *f* makes more compact plectonemic helices (smaller radius of the plectonemic helix). (*d*) Increased salt concentration makes more compact plectonemic helices. (*e*) Nucleation rate of the plectonemes as a function of force obtained from the two-phase model simulations for various l_p values. Each error bar represents the SD from simulation of 200 s. As a comparison, the experimentally measured nucleation rates of plectonemes are around 20 s^{-1} at 0.4 pN, and $<15 s^{-1}$ at 3.2 pN (Fig. 4 *D* in van Loenhout et al. (46)). (*f*) The mean lifetime of the individual plectoneme as a function of force and salt concentration. Note that only a single plectoneme is captured at $l_p = 21$ nm and $f = 3.2$ pN in simulations (nucleation and annihilation, however, need multiple plectonemes). Each error bar represents the standard deviation obtained from a 200-s simulation trajectory. In comparison, the experimental values of the mean plectoneme lifetime are 0.1 s at 0.4 pN and 1 s and above at 3.2 pN (Fig. 4 *E* in van Loenhout et al. (46)). (*g*) A hopping event of a displacement of plectoneme for nearly 4 μm from 0.4 to 0.55 s (marked by dashed lines), corresponding to 12 kbp. (*h*) Hopping distance versus time for a plectoneme with contour length 1.75 μm under an external force 0.8 pN. The error bars were estimated from 13,000 independent hopping simulation events, indicating the SD. The slope of the fitting lines (green line) is 1.8 μm/s, close to the previous estimation 1.4 μm/s (see the SI of van Loenhout et al. (46)). (*i*) Energetic conversion during hopping (nucleation is, for example, at 80 ms). The total energy changes of hopping (black line) and the reversed (complementary to hopping) process (dashed line) are also shown in the inset.

model of DNA supercoiling. To establish such a model, we demonstrate the fast dynamics of torque equilibrium within the S and P (plectonemic) phases, identify the phase boundaries as slow observables, and derive the energetics associated with the slow observables. By comparing with the WLC model, we have shown that the two-phase dynamic model provides a physically justified and computationally efficient way in representing DNA supercoiling dynamics. The model is particularly suited for studying plectoneme dynamics from milliseconds to seconds. Correspondingly, we have demonstrated the plectoneme dynamics, e.g., diffusion and hopping, consistently with measurements from single-molecule experiments (46,85,86).

To probe the timescale separation, we have investigated the dynamics of torque approaching to equilibrium within the S and P phases (intra-phase equilibrium), respectively.

Based on the WLC model, the internal torque transports as twist angle propagates within the S phase. Similarly, by introducing an effective twist angle of the plectonemic helix, the torque propagation within the P phase can be described. Such analyses are confirmed by numerical simulations based on the dWLC method, consistently showing that the torque transport is fast, compared to the dynamics of phase boundary.

Accordingly, we choose the the boundaries of the S and P phases as observables to describe the slow dynamics. Based on the interphase torque equilibrium, one can then derive the free energy associated with the collective phase boundaries and the corresponding equation of motion via the Langevin dynamics. In addition, one can add or delete a plectoneme via the MC procedures depending on the system energetics.

To compare the two-phase model with the dWLC method, we tested at a constant rate of supercoil accumulation, $\Delta Lk = 10$ per second, comparable to the RNA polymerization rate during transcription elongation (i.e., $\sim$ 100 bp per second) (23,82), and both intra-phase and interphase relaxations are all reached. Thus, supercoiling accumulation during transcription seems to be a quasi-static process. The discontinuities on torque and extension curves are reproduced by the two-phase dynamic model, reflecting the buckling transition during plectoneme nucleation (48,54–56,73,74). The advantage of the two-phase dynamic model of DNA supercoiling comes from its trivial computational cost as we only deal with the slow degrees of freedom of the system. Besides, we performed simulations of plectoneme growth under a constant torque since some studies treat RNAPs as a torsional motor with a constant torque (83). We accordingly determined slithering frictional coefficient by calibrating with the dWLC method.

With the two-phase model, we described the DNA supercoiling dynamics as being measured experimentally (46) and reproduced the plectoneme diffusion and hopping. The plectoneme diffusion coefficient is about 0.1–0.2 $\mu m^2/s$ under the regular salt concentration, decreasing slightly with the stretching force. Large force indeed makes the plectoneme more compact, which increases the friction for the slithering of parallel segments of the plectonemes. Hopping event is associated with nucleation and vanishing of plectonemes. Large stretching force suppresses the nucleation, as the force increases the energy penalty for forming a loop. Similar to the large stretching force, strong ionic strength results in compact plectonemes because of the ability of ions to screen the electrostatic repulsion between segments in plectonemes (46,80). The compact plectonemes thus have increased stabilities. Accordingly, large force or strong ionic strength can prolong the mean lifetime of the individual plectoneme, and consequently suppress the hopping capability. Moreover, on average, hopping distance scales linearly with hopping time and propagates faster than diffusion. Indeed, hopping is accompanied by significant energetic exchange between two phases, whereas the total energetic change of the coexistence phases is as small as thermal fluctuations.

Recent experiments reveal the long-distance cooperative and antagonistic dynamics between multiple RNAPs (20). In the cooperative case as RNAPs move toward the same direction, positive and negative supercoils are generated and then canceled with each other between adjacent RNAPs, which make the multiple RNAPs with similar transcription elongation speeds. Upon promoter repression or divergently transcribed genes, however, as RNAPs switch their behaviors from collaborative to antagonistic (i.e., moving opposite to each other), the supercoils build up between adjacent ones. Accordingly, the DNA supercoiling dynamics between the adjacent RNAPs can be described by the two-phase model, which then helps to explain how long-distance coordination arises among multiple RNAPs.

DNA supercoiling also facilitates the site juxtaposition of two distal DNA sites by slithering opposing segments of the interwound superhelix or bending DNA to coil (30,33,87,88). It consequently promotes transcription factor protein binding via intersegment transfer to possibly impact the gene expression (31,89,90). As we have seen, slithering motion of the segments in a plectonemic helix is accompanied with plectoneme diffusion. Combining plectoneme diffusion with faster hopping may offer a highly efficient mechanism for achieving site juxtaposition over long-range DNA. Such mechanisms can be explored by employing our two-phase dynamics of the DNA supercoiling.

In biological context, the sequence-dependent mechanical features and the intrinsic curvature of DNA may favor the plectonemes and nucleation loops at particular positions, preventing plectonemes from randomly diffusing and nucleating along DNA (60,91,92). The sequence effects on mechanical parameters, such as the bending persistence length and torsional persistence length, can be incorporated numerically in the two-phase dynamic model. How the DNA curvature and/or local variations in the bending and torsional stiffnesses impact the plectonemes can be a topic of further research.

SUPPORTING MATERIAL

Supporting material can be found online at https://doi.org/10.1016/j.bpj.2022.01.001.

AUTHOR CONTRIBUTIONS

J.Y. and B.W. designed the research. B.W. carried out all simulations and analyzed the data. B.W. and J.Y. wrote the article.

ACKNOWLEDGMENTS

This work has been supported by NSFC Grant #11775016 and #11635002. J.Y. has been supported by the CMCF of UCI via NSF DMS 1763272 and the Simons Foundation grant #594598 and start-up fund from UCI. We

acknowledge the computational support from the Beijing Computational Science Research Center (CSRC). Thanks to Dr Xinliang Xu for discussions on the work.

REFERENCES

1. Vinograd, J., J. Lebowitz, and R. Watson. 1968. Early and late helix-coil transitions in closed circular DNA the number of superhelical turns in polyoma DNA. *J. Mol. Biol.* 33:173–197.
2. Bates, A. D., and A. Maxwell. 2005. DNA Topology. Oxford University Press.
3. Fuller, F. B. 1971. The writhing number of a space curve. *Proc. Natl. Acad. Sci. U S A.* 68:815–819.
4. Koster, D. A., A. Crut, …, N. H. Dekker. 2010. Cellular strategies for regulating DNA supercoiling: a single-molecule perspective. *Cell.* 142:519–530.
5. Lavelle, C. 2014. Pack, unpack, bend, twist, pull, push: the physical side of gene expression. *Curr. Opin. Genet. Dev.* 25:74–84.
6. Dixon, J. R., S. Selvaraj, …, B. Ren. 2012. Topological domains in mammalian genomes identified by analysis of chromatin interactions. *Nature.* 485:376–380.
7. Glinsky, G. 2015. Rapidly evolving in humans topologically associating domains. *arXiv*, preprint arXiv:1507.05368.
8. Stadhouders, R., G. J. Filion, and T. Graf. 2019. Transcription factors and 3D genome conformation in cell-fate decisions. *Nature.* 569:345–354.
9. Naughton, C., N. Avlonitis, …, N. Gilbert. 2013. Transcription forms and remodels supercoiling domains unfolding large-scale chromatin structures. *Nat. Struct. Mol. Biol.* 20:387.
10. Gilbert, N., and J. Allan. 2014. Supercoiling in DNA and chromatin. *Curr. Opin. Genet. Dev.* 25:15–21.
11. Corless, S., and N. Gilbert. 2016. Effects of DNA supercoiling on chromatin architecture. *Biophys. Rev.* 8:245–258.
12. Postow, L., C. D. Hardy, …, N. R. Cozzarelli. 2004. Topological domain structure of the Escherichia coli chromosome. *Genes Dev.* 18:1766–1779.
13. Liu, L. F., and J. C. Wang. 1987. Supercoiling of the DNA template during transcription. *Proc. Natl. Acad. Sci. U S A.* 84:7024–7027.
14. Ma, J., L. Bai, and M. D. Wang. 2013. Transcription under torsion. *Science.* 340:1580–1583.
15. Chong, S., C. Chen, …, X. S. Xie. 2014. Mechanism of transcriptional bursting in bacteria. *Cell.* 158:314–326.
16. Burnier, Y., J. Dorier, and A. Stasiak. 2008. DNA supercoiling inhibits DNA knotting. *Nucleic Acids Res.* 36:4956–4963.
17. Schvartzman, J. B., M.-L. Martínez-Robles, …, D. B. Krimer. 2013. The benefit of DNA supercoiling during replication. *Biochem. Soc. Trans.* 41:646–651.
18. Hirano, T. 2000. Chromosome cohesion, condensation, and separation. *Annu. Rev. Biochem.* 69:115–144.
19. Strick, T. R., T. Kawaguchi, and T. Hirano. 2004. Real-time detection of single-molecule DNA compaction by condensin I. *Curr. Biol.* 14:874–880.
20. Kim, S., B. Beltran, …, C. Jacobs-Wagner. 2019. Long-distance cooperative and antagonistic RNA polymerase dynamics via DNA supercoiling. *Cell.* 179:106–119.
21. Teves, S. S., and S. Henikoff. 2014. DNA torsion as a feedback mediator of transcription and chromatin dynamics. *Nucleus.* 5:211–218.
22. Tantale, K., F. Mueller, …, E. Bertrand. 2016. A single-molecule view of transcription reveals convoys of RNA polymerases and multi-scale bursting. *Nat. Commun.* 7:1–14.
23. Jing, X., P. Loskot, and J. Yu. 2018. How does supercoiling regulation on a battery of RNA polymerases impact on bacterial transcription bursting? *Phys. Biol.* 15:066007.
24. Kimura, K., and T. Hirano. 1997. ATP-dependent positive supercoiling of DNA by 13S condensin: a biochemical implication for chromosome condensation. *Cell.* 90:625–634.
25. Swedlow, J. R., and T. Hirano. 2003. The making of the mitotic chromosome: modern insights into classical questions. *Mol. Cell.* 11:557–569.
26. Seol, Y., and K. C. Neuman. 2016. The dynamic interplay between DNA topoisomerases and DNA topology. *Biophys. Rev.* 8:101–111.
27. Ma, J., and M. Wang. 2014. Interplay between DNA supercoiling and transcription elongation. *Transcription.* 5:e28636.
28. Ma, J., and M. D. Wang. 2014. RNA polymerase is a powerful torsional motor. *Cell Cycle.* 13:337.
29. Fuller, F. B. 1978. Decomposition of the linking number of a closed ribbon: a problem from molecular biology. *Proc. Natl. Acad. Sci. U S A.* 75:3557–3561.
30. Parker, C. N., and S. E. Halford. 1991. Dynamics of long-range interactions on DNA: the speed of synapsis during site-specific recombination by resolvase. *Cell.* 66:781–791.
31. Liu, Y., V. Bondarenko, …, V. M. Studitsky. 2001. DNA supercoiling allows enhancer action over a large distance. *Proc. Natl. Acad. Sci. U S A.* 98:14883–14888.
32. Huang, J., T. Schlick, and A. Vologodskii. 2001. Dynamics of site juxtaposition in supercoiled DNA. *Proc. Natl. Acad. Sci. U S A.* 98:968–973.
33. Polikanov, Y. S., V. A. Bondarenko, …, V. M. Studitsky. 2007. Probability of the site juxtaposition determines the rate of protein-mediated DNA looping. *Biophys. J.* 93:2726–2731.
34. Marko, J. F. 1997. Supercoiled and braided DNA under tension. *Phys. Rev. E.* 55:1758.
35. Strick, T., J.-F. Allemand, …, V. Croquette. 1999. Phase coexistence in a single DNA molecule. *Phys. A Stat. Mech. Appl.* 263:392–404.
36. Ghatak, A., and L. Mahadevan. 2005. Solenoids and plectonemes in stretched and twisted elastomeric filaments. *Phys. Rev. Lett.* 95:057801.
37. Marko, J. F. 2007. Torque and dynamics of linking number relaxation in stretched supercoiled DNA. *Phys. Rev. E.* 76:021926.
38. Forte, G., M. Caraglio, …, E. Orlandini. 2019. Plectoneme dynamics and statistics in braided polymers. *Phys. Rev. E.* 99:052503.
39. Marko, J. F., and E. D. Siggia. 1994. Fluctuations and supercoiling of DNA. *Science.* 265:506–508.
40. Bustamante, C., J. Marko, …, S. Smith. 1994. Entropic elasticity of λ-phage DNA. *Science.* 265:1599–1600.
41. Strick, T. R., J.-F. Allemand, …, V. Croquette. 1996. The elasticity of a single supercoiled DNA molecule. *Science.* 271:1835–1837.
42. Strick, T., J.-F. Allemand, …, V. Croquette. 1998. Behavior of supercoiled DNA. *Biophys. J.* 74:2016–2028.
43. Bustamante, C., S. B. Smith, …, D. Smith. 2000. Single-molecule studies of DNA mechanics. *Curr. Opin. Struct. Biol.* 10:279–285.
44. Strick, T., J.-F. Allemand, …, D. Bensimon. 2000. Twisting and stretching single DNA molecules. *Prog. Biophys. Mol. Biol.* 74:115–140.
45. Koster, D. A., V. Croquette, …, N. H. Dekker. 2005. Friction and torque govern the relaxation of DNA supercoils by eukaryotic topoisomerase IB. *Nature.* 434:671–674.
46. van Loenhout, M. T., M. De Grunt, and C. Dekker. 2012. Dynamics of DNA supercoils. *Science.* 338:94–97.
47. Bustamante, C., Z. Bryant, and S. B. Smith. 2003. Ten years of tension: single-molecule DNA mechanics. *Nature.* 421:423–427.
48. Forth, S., C. Deufel, …, M. D. Wang. 2008. Abrupt buckling transition observed during the plectoneme formation of individual DNA molecules. *Phys. Rev. Lett.* 100:148301.
49. Marko, J. F., and E. D. Siggia. 1995. Stretching DNA. *Macromolecules.* 28:8759–8770.
50. Marko, J., and E. Siggia. 1995. Statistical mechanics of supercoiled DNA. *Phys. Rev. E.* 52:2912.

51. Moroz, J. D., and P. Nelson. 1997. Torsional directed walks, entropic elasticity, and DNA twist stiffness. *Proc. Natl. Acad. Sci. U S A.* 94:14418–14422.

52. Phillips, R. R. B., J. Kondev, …, H. Garcia. 2009. Physical Biology of the Cell. Garland Science.

53. Marko, J. F. 1998. DNA under high tension: overstretching, undertwisting, and relaxation dynamics. *Phys. Rev. E.* 57:2134.

54. Daniels, B. C., and J. P. Sethna. 2011. Nucleation at the DNA supercoiling transition. *Phys. Rev. E.* 83:041924.

55. Marko, J. F., and S. Neukirch. 2012. Competition between curls and plectonemes near the buckling transition of stretched supercoiled DNA. *Phys. Rev. E.* 85:011908.

56. Emanuel, M., G. Lanzani, and H. Schiessel. 2013. Multiplectoneme phase of double-stranded DNA under torsion. *Phys. Rev. E.* 88:022706.

57. Mitchell, J. S., and S. A. Harris. 2013. Thermodynamics of writhe in DNA minicircles from molecular dynamics simulations. *Phys. Rev. Lett.* 110:148105.

58. Mitchell, J., C. Laughton, and S. A. Harris. 2011. Atomistic simulations reveal bubbles, kinks and wrinkles in supercoiled DNA. *Nucleic Acids Res.* 39:3928–3938.

59. Irobalieva, R. N., J. M. Fogg, …, L. Zechiedrich. 2015. Structural diversity of supercoiled DNA. *Nat. Commun.* 6:1–11.

60. Matek, C., T. E. Ouldridge, …, A. A. Louis. 2015. Plectoneme tip bubbles: coupled denaturation and writhing in supercoiled DNA. *Sci. Rep.* 5:7655.

61. Sutthibutpong, T., C. Matek, …, S. A. Harris. 2016. Long-range correlations in the mechanics of small DNA circles under topological stress revealed by multi-scale simulation. *Nucleic Acids Res.* 44:9121–9130.

62. Hirsh, A. D., M. Taranova, …, N. Perkins. 2013. Structural ensemble and dynamics of toroidal-like DNA shapes in bacteriophage ϕ29 exit cavity. *Biophys. J.* 104:2058–2067.

63. Dans, P. D., J. Walther, …, M. Orozco. 2016. Multiscale simulation of DNA. *Curr. Opin. Struct. Biol.* 37:29–45.

64. Goyal, S., N. C. Perkins, and C. L. Lee. 2005. Nonlinear dynamics and loop formation in Kirchhoff rods with implications to the mechanics of DNA and cables. *J. Comput. Phys.* 209:371–389.

65. Lillian, T. D., M. Taranova, …, N. Perkins. 2011. A multiscale dynamic model of DNA supercoil relaxation by topoisomerase IB. *Biophys. J.* 100:2016–2023.

66. Hirsh, A. D., T. D. Lillian, …, N. Perkins. 2013. A model for highly strained DNA compressed inside a protein cavity. *J. Comput. Nonlinear Dyn.* 8:031001.

67. Vologodskii, A. 2006. Simulation of equilibrium and dynamic properties of large DNA molecules. *In* Computational Studies of RNA and DNA. Springer, pp. 579–604.

68. Vologodskii, A. V., S. D. Levene, …, N. R. Cozzarelli. 1992. Conformational and thermodynamic properties of supercoiled DNA. *J. Mol. Biol.* 227:1224–1243.

69. Klenin, K. V., A. V. Vologodskii, …, M. D. Frank-Kamenetskii. 1991. Computer simulation of DNA supercoiling. *J. Mol. Biol.* 217:413–419.

70. Klenin, K., H. Merlitz, and J. Langowski. 1998. A Brownian dynamics program for the simulation of linear and circular DNA and other wormlike chain polyelectrolytes. *Biophys. J.* 74:780–788.

71. Bell, D., P. Selokar, and T. D. Lillian. 2012. Simulation of plectonemic supercoil diffusion along extended DNA by brownian dynamics. *Biophys. J.* 102:276a.

72. Babamohammadi, S., and T. D. Lillian. 2020. Traveling salesman finds random walk: a curve reconstruction algorithm for supercoiled DNA. *Biophys. J.* 119:2517–2523.

73. Walker, P. U., W. Vanderlinden, and J. Lipfert. 2018. Dynamics and energy landscape of DNA plectoneme nucleation. *Phys. Rev. E.* 98:042412.

74. Ott, K., L. Martini, …, U. Gerland. 2020. Dynamics of the buckling transition in double-stranded DNA and RNA. *Biophys. J.* 118:1690–1701.

75. Wocjan, T., K. Klenin, and J. Langowski. 2009. Brownian dynamics simulation of DNA unrolling from the nucleosome. *J. Phys. Chem. B.* 113:2639–2646.

76. Ivenso, I. D., and T. D. Lillian. 2016. Simulation of DNA supercoil relaxation. *Biophys. J.* 110:2176–2184.

77. Wada, H., and R. R. Netz. 2009. Plectoneme creation reduces the rotational friction of a polymer. *Europhys. Lett.* 87:38001.

78. Fasnacht, M., R. H. Swendsen, and J. M. Rosenberg. 2004. Adaptive integration method for Monte Carlo simulations. *Phys. Rev. E.* 69:056704.

79. Zhang, C., and J. Ma. 2010. Enhanced sampling and applications in protein folding in explicit solvent. *J. Chem. Phys.* 132:244101.

80. Rybenkov, V. V., A. V. Vologodskii, and N. R. Cozzarelli. 1997. The effect of ionic conditions on DNA helical repeat, effective diameter and free energy of supercoiling. *Nucleic Acids Res.* 25:1412–1418.

81. Neukirch, S., and J. F. Marko. 2011. Analytical description of extension, torque, and supercoiling radius of a stretched twisted DNA. *Phys. Rev. Lett.* 106:138104.

82. Thomen, P., P. J. Lopez, and F. Heslot. 2005. Unravelling the mechanism of RNA-polymerase forward motion by using mechanical force. *Phys. Rev. Lett.* 94:128102.

83. Mielke, S. P., W. H. Fink, …, C. J. Benham. 2004. Transcription-driven twin supercoiling of a DNA loop: a Brownian dynamics study. *J. Chem. Phys.* 121:8104–8112.

84. Mosconi, F., J. F. Allemand, …, V. Croquette. 2009. Measurement of the torque on a single stretched and twisted DNA using magnetic tweezers. *Phys. Rev. Lett.* 102:078301.

85. Shashkova, S., and M. C. Leake. 2017. Single-molecule fluorescence microscopy review: shedding new light on old problems. *Biosci. Rep.* 37:BSR20170031.

86. Sheinin, M. Y., and M. D. Wang. 2012. A DNA twist diffuses and hops. *Science.* 338:56–57.

87. Oram, M., J. F. Marko, and S. E. Halford. 1997. Communications between distant sites on supercoiled DNA from non-exponential kinetics for DNA synapsis by resolvase. *J. Mol. Biol.* 270:396–412.

88. Marko, J. F. 1997. The internal 'slithering'dynamics of supercoiled DNA. *Phys. A Stat. Mech. Appl.* 244:263–277.

89. van den Broek, B., M. A. Lomholt, …, G. J. Wuite. 2008. How DNA coiling enhances target localization by proteins. *Proc. Natl. Acad. Sci. U S A.* 105:15738–15742.

90. Lomholt, M. A., B. van den Broek, …, R. Metzler. 2009. Facilitated diffusion with DNA coiling. *Proc. Natl. Acad. Sci. U S A.* 106:8204–8208.

91. Dittmore, A., S. Brahmachari, …, K. C. Neuman. 2017. Supercoiling DNA locates mismatches. *Phys. Rev. Lett.* 119:147801.

92. Desai, P. R., S. Brahmachari, …, K. C. Neuman. 2020. Coarse-grained modelling of DNA plectoneme pinning in the presence of base-pair mismatches. *Nucleic Acids Res.* 48:10713–10725.